HHS Public Access

Author manuscript

Placenta. Author manuscript; available in PMC 2022 October 01.

Published in final edited form as:

Placenta. 2021 October ; 114: 124–132. doi:10.1016/j.placenta.2021.08.058.

Quantitative T_1 and T_2 mapping by Magnetic Resonance Fingerprinting (MRF) of the placenta before and after maternal hyperoxia

Jeffrey N Stout[a], **Congyu Liao**[b], **Borjan Gagoski**[a], **Esra Abaci Turk**[a], **Henry A. Feldman**[c], **Carolina Bibbo**[d], **William H Barth Jr.**[e], **Scott A Shainker**[f], **Lawrence L Wald**[b], **P. Ellen Grant**[*,a], **Elfar Adalsteinsson**[*,g]

[a]Fetal and Neonatal Neuroimaging and Developmental Science Center, Boston Children's Hospital, Boston, MA, 02115.

[b]Athinoula A. Martinos Center for Biomedical ImagingMassachusetts General Hospital, Boston, MA, 02129.

[c]Boston Children's Hospital, Boston, MA, 02115.

[d]Brigham and Women's Hospital, Division of Maternal-Fetal Medicine, Boston, MA, 02115.

[e]Maternal-Fetal Medicine, Obstetrics and Gynecology, Massachusetts General Hospital, Boston, MA, USA, 02114.

[f]Maternal-Fetal Medicine, Obstetrics and Gynecology, Beth Israel Deaconess Medical Center, Boston, MA, USA, 02115.

[g]Electrical Engineering and Computer Science; Institute for Medical Engineering and Science, Massachusetts Institute of Technology, Cambridge, MA, 02139, USA.

Abstract

Introduction: MR relaxometry has been used to assess placental exchange function, but methods to date are not sufficiently fast to be robust to placental motion. Magnetic resonance fingerprinting (MRF) permits rapid, voxel-wise, intrinsically co-registered T_1 and T_2 mapping. After characterizing measurement error, we scanned pregnant women during air and oxygen breathing to demonstrate MRF's ability to detect placental oxygenation changes.

Corresponding author: Jeffrey N Stout, jeffrey.stout@childrens.harvard.edu, Boston Children's Hospital, Neonatal Neuroimaging BCH3181, 300 Longwood Ave. Boston, MA, 02115.

[*]PEG and EA contributed equally to this work.

Author Contributions and Conflicts of Interest

All authors declare that they have seen and approved the final version. They have no conflicts of interest to declare. JNS designed the study, collected and analyzed the data and wrote the manuscript. CL developed and implemented the MRF sequence and reconstruction pipeline. BG conducted scans and provided technical support for sequence installation. EAT conducted scans and helped develop the manuscript. HAF oversaw the development of statistical models and analysis. CB, WHB, SS recruited subjects from among their patients. LLW oversaw phantom construction and sequence development. EG and EA oversaw project design, data analysis, and manuscript preparation.

Methods: The accuracy of FISP-based, sliding-window reconstructed MRF was tested on phantoms.MRF scans in 9-s breath holds were acquired at 3T in 31 pregnant women during air and oxygen breathing. A mixed effects model was used to test for changes in placenta relaxation times between physiological states, to assess the dependency on gestational age (GA), and the impact of placental motion.

Results: MRF estimates of known phantom relaxation times resulted in mean absolute errors for T_1 of 92 ms (4.8%), but T_2 was less accurate at 16 ms (13.6%). During normoxia, placental T_1=1825±141 ms (avg±standard deviation) and T_2=60±16 ms (gestational age range 24.3-36.7, median 32.6 weeks). In the statistical model, placental T_2 rose and T_1 remained contant after hyperoxia, and no GA dependency was observed for T_1 or T_2.

Discussion: Well-characterized, motion-robust MRF was used to acquire T_1 and T_2 maps of the placenta. Changes with hyperoxia are consistent with a net increase in oxygen saturation. Toward the goal of whole-placenta quantitative oxygenation imaging over time, we aim to implement 3D MRF with integrated motion correction to improve T_2 accuracy.

Keywords

placenta; magnetic resonance fingerprinting; pregnancy; T_1; T_2; relaxometry

Introduction

MRI techniques to measure placental function could be important clinical tools to diagnose placental etiologies of fetal growth restriction (FGR) that complicates roughly 10% of all pregnancies and is a leading cause of perinatal morbidity and mortality [1]. Current ultrasound-based methods are not sufficiently specific to determine when placental dysfunction is causing FGR [2,3]. MRI is sensitive to blood oxygenation and methods relying on T_2* and T_1 contrast have detected differences between placentas of typically developing and FGR pregnancies [4,5]. However, methods for accurate measurements of placental oxygen exchange function in singleton pregnancies that are sufficiently robust to fetal motion for clinical use have yet to be validated.

The first attempts at MRI-based placental oxygen exchange assessment used BOLD (T_2*-weighted) imaging to visualize the oxygenation state changes between maternal air and oxygen breathing [6,7]. It was demonstrated that placental dysfunction affected baseline BOLD imaging, contributed to observed changes with hyperoxia [8], and that the signal dynamics during maternal hyperoxia were highly correlated with outcomes in discordant monozygotic twins [5]. But when attempting to use these techniques to predict outcomes in singleton pregnancies a host of confounding variables have been identified that has so far limited the clinical application of T_2* imaging with hyperoxia [9]. One of the important factors in this lack of specificity is that BOLD imaging and T_2* mapping are not fundamentally quantitative with respect to blood oxygen saturation. The BOLD signal is directly related to the deoxygenated hemoglobin concentration within an imaging voxel, but even in the brain with its single circulation this concentration is an integrated signal that depends on blood volume, blood flow, and blood oxygen saturation that are difficult to disambiguate [10]. T_2* is affected by local magnetic field inhomogeneities, whereas T_2 is

an intrinsic tissue property. Techniques to quantify placental blood oxygenation that are not sensitive to field inhomogeneities could offer more precise assessments of placental oxygen exchange function.

The T_1 and T_2 of blood mostly depend on oxygen saturation (SO_2), but also on hematocrit (Hct). T_1 is also sensitive to pO_2, with a linear decrease in T_1 at pO_2 values exceeding full hemoglobin saturation (when there is a larger fraction of dissolved oxygen in blood unattached to hemoglobin) [11]. Combining T_1 and T_2 estimates of blood permits the quantification of both SO_2 and Hct [12]. Furthermore the relationship between T_1, T_2 and SO_2 is different for fetal and adult blood [13-15]. Though it is impossible to estimate all the relevant physiological parameters related to oxygen exchange function (blood volumes and oxygen saturations for both maternal and fetal compartments) on a voxelwise basis from T_1 and T_2 mapping alone, there is already evidence that T_1 and T_2* combined permit better prediction of FGR than either alone [4]. T_1 and T_2 mapping combined with additional measures of hemodynamics, may make it possible to discriminate between maternal and fetal blood compartments, or to assess voxel-wise admixture during maternal oxygen breathing. However, routine use of combined T_1 and T_2 mapping has been limited primarily by placental motion.

Currently, the most practical approach to motion mitigation during placental imaging is to acquire data as quickly as possible in order to “freeze” motion. Thus relaxometry techniques with short acquisition times are favored. For example, one study that used T_1 mapping to study placental oxygenation relied on a technique that takes approximately 3 minutes to acquire an initial map with four images at different inversion times (TI), and then performed dynamic T_1-imaging by acquiring only one image at a fixed TI every 12 seconds [16]. Motion between images was handled by rejecting data where motion occurred which affected 10/14 subjects [16]. T_2 mapping of the placenta has been performed using various single-shot, multi-TE, approaches where scan times were between 4-22 seconds per slice [17,18]. Motion between TEs was visualized and rejected. Thus, given the challenges of motion in placental imaging, a relatively fast acquisition of T_1 and T_2 maps would be a major breakthrough, and if these maps were intrinsically coregistered this could eventually enable voxel-wise estimation of SO_2 and Hct over time.

A new method of T_1 and T_2 mapping called magnetic resonance fingerprinting (MRF) has been proposed [19] where parameter maps can be acquired more quickly than with other methods [8,16,20], and maps are generated for each parameter from the same set of acquisitions reducing the challenge of misalignment. Here we evaluate the performance of a FISP-based MRF implementation [21] for placental imaging in phantoms, and then provide results from 31 placentas of typically developing fetuses. This work builds on our initial report [22] by employing sliding-window reconstruction to maintain parameter estimation accuracy with a shorter 9-second acquisition [23]. The shorter scan fits easily within a maternal breath hold, and the reconstruction scheme allows motion-corrupted acquisitions to be detected thereby improving T_1 and T_2 quantification accuracy. Using both a National Institute of Standards and Technology (NIST) MRI System Phantom and an anthropomorphic 22-week pregnant abdomen phantom [24], we studied the overall quantification accuracy of our MRF implementation. To assess MRF’s ability to characterize

placental oxygen changes over time, in vivo T_1 and T_2 mapping was conducted both at baseline and during maternal hyperoxia as maternal hyperoxia is thought to alter placental relaxation times [4].

Methods

Human scanning was IRB approved with informed consent obtained from all subjects. Pregnant subjects with typically developing fetuses between 24-40 weeks gestational age (GA) and maternal body mass index less than 32 were recruited from the community and from among patients seen at Massachusetts General Hospital, Beth Israel Deaconess Medical Center, and Brigham and Women's Hospital (see Table 1 [25]). Exclusion criteria were chromosomal anomalies or known genetic disorders, congenital heart disease, major congenital malformation. All human subject scans took place at Boston Children's Hospital and phantom scanning at the Athinoula A. Martinos Center for Biomedical Imaging at Massachusetts General Hospital on Siemens Skyra 3T MRI scanners (Siemens Healthineers, Erlangen, Germany). In both locations we used the Siemens spine array and 34-channel flexible body coil. Subjects were scanned in the left lateral position and SAR did not exceed 2 W/kg at any time.

Phantom and in vivo data acquisition

Two phantoms were used to characterize the performance of the MRF sequence that we implemented. First, we used the NIST MRI System Phantom (https://collaborate.nist.gov/mriphantoms/bin/view/MriPhantoms/MRISystemPhantom) [26]. Reference NMR relaxation measurements from each of the doped samples at 3T and 293 K have been previously reported [26] and are within 2.5% of the values measured by single echo spin-echo based techniques presented in [27]. Second, we used a 22-week anthropomorphic pregnant abdomen phantom [24]. In this phantom compartments resembling the uterus, placenta, fetus, fetal brain and cerebral ventricles were filled with water or agar doped with NaCl and $GdCl_3$ to achieve relaxation times resembling those observed in vivo. The 22-week phantom better demonstrates the magnetic field variation across the abdomen at 3T and contains T_1 and T_2 pairs that are closer to the values found in fetal tissues.

Ground truth relaxation times for the 22-week anthropomorphic phantom were determined using reference methods. For T_1, we used an inversion recovery spin echo (IR-SE) method with repetition time (TR) = 10000 ms, echo time (TE) = 12 ms, inversion time = 100, 500, 1100, 2200, 4600, voxel size = 2.8x2.8x4 mm^3, field of view (FOV) = 360 mm, and total acquisition (TA) time = 108 min. For T_2, we used a single-echo spin echo (SE) method with TR=4000 ms, TE = 25, 50, 75, 100, 200, 300 ms, voxel size = 3.125 x 3.125 x 4 mm^3, FOV=400 mm, TA=39 min.

MRF acquisitions were based on a previously implemented FISP variant of MRF [21,23] that was modified to include a large FOV spiral readout for use on the pregnant abdomen. Following a 5.12 ms hyperbolic-tangent-modulated adiabatic inversion pulse for homogeneous inversion across the FOV, 720 acquisitions were made as the TR was varied between 12 and 12.81 ms following a Perlin noise pattern, and flip angles (FA) were sinusoidally varied between 3-78°, TE=2.7 ms (Supplementary Figure S1 A), and TA=9 s.

Data acquisition was by a constant density spiral trajectory with zero moment nulling, where 30 interleaves each rotated by 12° would give fully sampled k-space, resolution=3x3x4 mm^3, FOV=390 mm (Supplementary Figure S1 A).

Transmit field heterogeneity (B_1^+) maps (Supplementary Figure S1) were obtained using a saturation turboflash sequence [28] with TR/TE = 20000/2.06 ms, voxel size = 2.8x2.8x4.0 mm^3, FOV=360 mm, matrix size = 128x128, flip angle = 8°, TA=40 s for phantom scans, and TR/TE=15000/1.97 ms, voxel size = 6x6x5 mm^3, FOV=384 mm, matrix size = 64x64, flip angle = 8°, TA=30 s for human scans.

Pregnant women (N = 31, 24.3-36.7 weeks gestational age) were scanned during breath hold after breathing room air and after breathing 100% oxygen (15 L/min flow rate) for 5 or 10 minutes depending on the specific protocol being used. Subjects were scanned in the left lateral position. We selected our imaging plane as the maternal-transversal slice with the most placental coverage. The transversal constraint was to operate within the technical limitations of our MRF implementation that could not acquire oblique slices. B_1^+ maps were acquired immediately after the final MRF acquisition. For some subjects (N = 25) we acquired three consecutive MRF scans (with 15 s pause in between for a TA = 57 s) in each physiological state in order to estimate repeatability and to improve the chance of collecting at least one motion free acquisition.

T_1 and T_2 parameter map generation

For reference methods, T_1 maps were determined by fitting $S(TI) = a - be^{-TI/T1}$ to each voxel using the methods described in [29]. T_2 maps were determined by fitting $S(TE) = ae^{-TE/T2}$ to each voxel of the SE data. The median and interquartile range (IQR) of T_1 and T_2 were determined for regions of interest (ROI) drawn by hand for the compartments representing the maternal abdomen, placenta, amniotic fluid, fetal body, fetal brain (inset of Figure 2).

The sliding window reconstruction approach for determining MRF parameter maps was used following the methods described in [23], while also correcting for B_1^+ in homogeneity and slice profile imperfections using the approach detailed in Supplemental Information. Briefly, images from each TR were reconstructed then complex summed across windows of thirty time points to generate a series of “fully sampled” images. For each voxel, the signal time course was then matched to the appropriate mixed-contrast dictionary by selecting the entry with highest inner-product. A mixed-contrast dictionary was generated according to [23] using an extended phase graph simulation [30] for each T_1 and T_2 pair. The dictionary resolution, denoted as min:step:max, was T_1 = 20:20:3000, 3200:200:5000 ms, and T_2 = 10:2:140, 145:5:300, 310:12:1000, 1050:50:2000, 2100:100:4000 ms.

Region of interest analysis and statistical comparisons

ROIs were drawn by hand (JNS) from the proton density maps for both phantom and human imaging data after training from an experienced placental imaging researcher (EAT) and supervised by a board certified radiologist (PEG). For comparisons between MRF and other relaxation measurements, error in median T_1 or T_2 estimates for ROIs was determined by calculating the mean absolute error ($MAE = \sum(|T_{est} - T_{ref}|)/N$). Errors were summed

over ROI types for phantom measurements. Motion that occurred during each in vivo MRF acquisition was detected by visual review of the mixed-contrast images from the sliding window reconstruction (example movies provided in Supplemental Information). Motion was evaluated by two reviewers (JNS and EAT) and deemed present when the slice moved due to maternal repositioning, the placenta was observed to change shape or position, or fetal motion occurred adjacent to the placenta. The interrater reliability of this method was determined by calculating the percentage of agreement, and then all divergent calls were reconciled by discussion between the raters. Changes in relaxation due to maternal hyperoxia were determined using statistical analyses performed in Matlab®8.5, (MathWorks Inc., Natick, MA). We used a mixed-effects model of the median and IQR of parameter values within the ROIs for trials where we did not detect motion, with fixed effects for oxygen state (α_{O2}), linear effect for gestational age (β), and a random effect for subject identification to account for within-subject correlation in those with multiple measurements. We also modeled all trials (motion and no motion) while including an additional fixed effect for motion (α_{motion}) in order to assess its effect on T_1 and T_2 estimates in vivo.

Results

MRF performance determined using NIST phantom

Bland-Altman analyses of the B_1^+ and slice profile corrected MRF compared to reference relaxation times for the NIST phantom are shown in Figure 1, and these values are tabulated in Supplementary Table S1. The temperature of the NIST phantom was 294 K at the time of scan. The 95% limits of agreement comparing MRF and ground truth relaxation times [26] are −26-80 ms for T1 and −44-58 ms for T_2. The MAE for the entire range of the NIST phantom is 29 ms (8%) for T_1 but worse for T2 at 16 ms (12%).

MRF performance determined using 22-week phantom

In Figure 2, example parameter maps from the 22-week pregnant abdomen phantom phantom are shown alongside a graphical presentation of the measured the$_1$ and T_2 values for select compartments in the 22-week phantom and NIST phantom. In the approximate range of relaxation times we observed for fetal tissues (T_1 = 1000 – 3000 ms and T_2 = 30 – 250 ms, gray rectangle in Figure 2 E) MAE for both phantoms combined was 92 ms (4.8%) for T_1, and, similar to NIST phantom, worse for T_2 at 16 ms (13.6%). MAE in the fetal range without B_1^+ and slice profde correction was worse for both T_1 and T_2 (125 ms (6.3%) and 90 ms (65.0%), respectively), which indicates the importance of these corrections. The contributions of each correction, B_1^+ and SPC individually, are visualized in Supplementary Figure S2. The amniotic fluid compartment is not shown in Figure 2E, but its ground truth T_1 and T_2, were 2506 (70) ms, and 1346 (155) ms, respectively, and MRF parameter estimate 2520 (40) ms and 730 (72) ms, respectively (median (IQR)).

MRF normoxia results

Supplementary Table S2 summarizes ROI-median T_1 and T_2 estimates collected for all subjects.

We successfully acquired motion-free MRF maps of the placenta during normoxia in 28/31 subjects with median GA of 32.6 and a range of 24.3-36.7 weeks. Interrater percentage agreement on motion calls was 95%. Raters reached unanimous consensus on all divergent cases after discussion. Example parameter maps are shown in Figures 3 and 4, with a motion corrupted example in Supplementary Figure S3. Histograms of the T_1 and T_2 estimates from the placental ROIs in each subject are given in Supplementary Figure S4. Figure 5 shows the median relaxation times from the ROI for each placenta during normoxia. Average placental T_1 = 1825±141 ms and T_2 = 60±16 ms (avg±standard deviation).

For three subjects we acquired MRF parameters maps from two different planes intersecting the placenta, in order to gauge the effect of positioning on our results. From the summary of values in Supplementary Table S3 it can be seen that there were significant differences ($P < 0.03$) between the two slices in only one case of placenta ROI T_1 estimates.

Statistical analyses of MRF data

Complete results from mixed-effects modeling are given in Table 2. For all 29 motion free observations of the placenta, we did not observe a significant change in T_1 after oxygen breathing ($P = 0.58$), but T_2 rose by 3 ms after hyperoxia ($P = 0.04$). We also found a decrease of 27 ms in the IQR of T_1 ($P = 0.01$) during hyperoxia. Placental measurement repeatability was estimated by standard deviations of the residual error, which were 65 ms and 7 ms for T_1 and T_2, respectively. Motion during the MRF acquisition appears to decrease T_2 estimates by 10 ms ($P < 0.01$), with no effect on median T_1.

Discussion

We implemented MRF-based relaxometry for placental imaging and characterized its measurement error before quantifying placental relaxation times in 31 pregnant women during air and oxygen breathing. Using phantoms with attributes similar to the pregnant abdomen (large FOV, B_1^+ heterogeneity, and T_1 and T_2 values in the correct ranges), we have determined the ultimate accuracy expected using FISP-based MRF with B_1^+ and slice profile correction (MAE for T_1 of 4.8% and for T_2 13.6%). Using a relaxometry method that is much faster than previous approaches [16-18], allowed the visualization and detection of motion over the 9-s acquisition, whilst acquiring intrinsically co-registered T_1 and T_2 maps. We observed placental T_1 and T_2 values during normoxia that were in good agreement with previously published results, and which showed no significant correlation between either T_1 or T_2 and GA. During maternal hyperoxia we observed an increased placental T_2, while T_1 remained constant, which to our knowledge [31], is the first report of an experiment using MRF to characterize an inducible physiological change.

Our implementation of corrected MRF performed well when compared to literature reports of other MRF implementations [19,21,27,32,33]. It is important to consider that the NIST phantom does not have many T_1 and T_2 pairings within the expected physiological range of fetal and placental tissues. Thus, although Figure 1 shows that MRF predominantly overestimated T_1 and T_2, Figure 2E shows that in the physiological range of fetal tissues, MRF biases were both positive and negative. To contextualize these biases, consider using T_1 and T_2 measurements to estimate blood oxygen saturation. A 5% error in the T_1 or T_2

measurement of blood with a hematocrit of 0.4, could lead to a maximum uncertainty in SO_2 of 15% [12]. Less than 5% error is a reasonable threshold for declaring MRF useful for quantifying oxygenation of blood in the placenta or fetus. MRF T_1 estimates have almost reached this threshold, but future work is needed to improve T_2 quantification accuracy.

Our MRF results for T_1 estimates of the placenta during normoxia were generally in agreement with previous studies [4,16,17,34]. One study at 3T reported T_1 estimates of 2031±58 ms (mean±standard deviation) for a cohort of nine subjects with a median GA = 28.5 (range 20.7-38.7) weeks, which used a respiratory gated inversion recovery with single shot fast spin echo method [34]. These results were higher than our own, but for a younger cohort. Some studies [17,35] have found that placental T_1 decreases with GA, whereas other studies, and our own, have found no evidence for this trend [4,16,34].

Studies of placental T_2 at 1.5T gave results that were higher than our own [17,36]. T_2 of the placenta may be lower at 3T, however, based on evidence from the liver and blood we expected this difference to be smaller than 10 ms [37]. Typical placental motion could affect the T_2 measurements in these previous studies, with acquisition schemes that took minutes, or motion more subtle than that rejected from our analysis could also depress our estimates (see discussion below). Though it is known that T_2* decreases with GA, which is likely driven by the decrease in placental oxygenation with GA [9,38], it remains unclear how changes to tissue morphology, known to have different, specific effects on T_2* and T_2 [39], affects T_2* and T_2 of the placenta. A prior observation of a significant negative correlation between T_2 and GA was for a cohort with a larger GA range than our study and our observed trend of −1 ms per week, is within the 95% confidence interval of that study [17].

The short acquisition time of MRF is well suited to monitor physiological changes through time, and our simultaneous observations of T_1 and T_2 of the placenta in two physiological states indicate the feasibility of including these measurements in future efforts to assess placental oxygen exchange function. T_1 and T_2 maps in conjunction with methods to account for blood volume changes and blood saturations entering and leaving the placenta (observations that are possible [18,40]), could potentially quantify absolute, voxelwise changes in placental oxygenation. As an illustration, if the observed change in T_2 originates from the fetal blood compartment (Hct = 0.5) and published calibrations between relaxation and blood oxygen saturation [13] hold for MRF sequences, the average T_2 we observe for the placenta (60 ms) would mean SO_2=67%, and the change (+2.8 ms) would mean the fetal saturation would increase to 68.3% during hyperoxia. This change is consistent with a previously observed relative 5.6% increase in umbilical vein T_2 during maternal hyperoxia [40], and observations of no or only small change in umbilical vein SO_2 with supplemental oxygen during labor [41]. Meanwhile the observed T_1 (1825 ms) that does not significantly change with hyperoxia, is slightly higher than the peak T_1 for blood at approximately pO_2 = 90 mmHg [42], which suggests that average pO_2 of the placenta is around 90 mmHg. This operating point is consistent with a diffusion-limited state where there is a large pO_2 gradient between maternal intervillous blood and fetal blood during hyperoxia, which has been observed via invasive sampling during labor [41].

Our observation of no change in placental T_1 with maternal hyperoxia contrasted with three previous studies that found a significant decrease [4,16,34]. These studies explained the decrease exclusively in terms of increasing dissolved oxygen, (i.e. pO_2). T_1 is sensitive to both SO_2 and pO_2. T_1 versus pO_2 peaks at SO_2 = 100%, and has a negative and linear relationship above that point [11,13,42]. A decrease in T_1 with maternal air breathing makes sense for only fully saturated maternal arterial blood, but many blood compartments in the placenta are less than fully saturated even during maternal hyperoxia [43]. A spatial average between compartments where T_1 increased alongside SO_2, and those where T_1 decreased with increased pO2 beyondm SO2=100%, could explain why we did not observe a change in T_1 with hyperoxia in the placenta. The liver, another dual circulation organ, also has shown no change in T_1 during hyperoxia [44].

It remains possible that measurement error contributes to the discrepancies between our MRF-based quantification and findings from other studies [4,16,34]. Our phantom observations suggested there may be different T_1 and T_2 biases in MRF estimates depending on the T_1 and T_2 operating point (see Figure 2E). For example, a T_2 overestimate during normoxia and an underestimate during hyperoxia could lead to a small net or even negative change in T_2 between the two states. We estimated the repeatability of our placental T_2 measurements to have a standard deviation of approximately 8 ms, which could also account for some inconsistency in the expected change with only 1-3 observations in each state. Finally, there were likely hemodynamic changes in the placenta associated with maternal hyperoxia that may affect the estimation accuracy of MRF. The placenta is over 50% blood by volume, and relaxed inflowing spins affect the net signal evolution [45]. Taken together, these observations specifically motivate further development of MRF-based T_2 estimation, perhaps using magnetization preparation pulses [46].

Data rejection appears to be an effective strategy for mitigating the effects of motion on the relatively fast MRF acquisitions, but motion continues to be a liability. Investigation on the adult brain and rigid phantoms have shown that the predominant effect of motion early in the MRF acquisition is a blurring of the T_1 map, and during the middle to end of the acquisition is an underestimate of the T_2 map [47]. Our data supports both observations (Supplementary Figure S3) Our data confirmed this underestimation due to motion in non-rigid objects such as the placenta. Though there have been efforts to correct for rigid body motion [48,49] as a step in the MRF reconstruction process, or for the repetitive motion of the heart [46,50], efforts to correct for non-rigid motion are limited [46]. 3D MRF sequences provide a framework that could address out of plane motion [51-53], but work is needed to correct for non-rigid motion that would be relevant for whole placenta imaging. We are considering whether spatiotemporally incoherent artefacts which underlie MRF may be undesirable when trying to perform motion correction, so we are in the process of evaluating other advanced relaxometry techniques, such as echo planar time-resolved imaging [54] and multi-inversion multi-echo spin and gradient echo, echo planar imaging [55] both of which may have the added benefit of more accurately quantifying T_2.

A final limitation of our study is that the MRF acquisition was a single 2D slice. This approach will not capture the full spatial heterogeneity of the placenta [56,57] nor guarantee that imaging has captured a representative portion of the organ. Our ROI-based observations

suggested this latter effect is minimal for the healthy placentas we studied here, and previous investigations of this possibility also demonstrated no average difference between ROIs on different imaging slices [16]. However, we recognize the value of whole placenta or whole uterus mapping for detecting lesions or to monitor volume changes with contractions [58]. These concerns motivate our interest in developing whole organ imaging using 3D MRF.

Using MRF, we successfully acquired relaxation time maps of the placenta in 28/31 pregnant women during normoxia, and observed a significant increase in T_2 with hyperoxia. By determining the method's measurement error in phantoms, and detecting and rejecting motion during the fast 9-s in vivo acquisition the T_1 and T_2 values of the placenta reported here are among the most well characterized to date. Toward robust quantification of placental blood oxygenation on a voxel-wise basis, future work will aim to provide whole placenta coverage, integrated motion correction, and improved T_2 quantification accuracy.

Supplementary Material

Refer to Web version on PubMed Central for supplementary material.

Acknowledgements

We would like to thank Filiz Yetisir, Huihui Ye and Bo Zhao for their help and suggestions when implementing the MRF acquisition and reconstruction. We also wish to thank our dedicated team of research assistants, Natalie Copeland, Gina Distefano, Elizabeth Holland and Cindy Zhou who recruited, consented and prepared our subjects for their scans. This work was supported by the National Institutes of Health [NIBIB R01EB017337, NICHD U01HD087211, NICHD R01HD100009 and NIBIB R01EB017219]

Funding sources

This work was supported by the National Institutes of Health [NIBIB R01EB017337, NICHD U01HD087211, NICHD R01HD100009, and NIBIB R01EB017219].

Abbreviations

B_1^+	transmit field heterogeneity
BOLD	blood oxygen level dependent
FOV	field of view
FGR	fetal growth restriction
GA	gestational age
Hct	hematocrit
IQR	interquartile range
MAE	mean absolute error
MRF	magnetic resonance fingerprinting
MRI	magnetic resonance imaging
ROI	region of interest

SO2	Blood oxygen saturation
TA	total acquisition
TE	echo time
TR	repetition time

References

[1]. Society for Maternal-Fetal Medicine (SMFM). Electronic address: pubs@smfm.org, Martins JG, Biggio JR, Abuhamad A, Society for Maternal-Fetal Medicine Consult Series #52: Diagnosis and management of fetal growth restriction: (Replaces Clinical Guideline Number 3, April 2012), Am. J. Obstet. Gynecol 223 (2020) B2–B17. 10.1016/j.ajog.2020.05.010.

[2]. Chauhan SP, Magann EF, Dohrety DA, Ennen CS, Niederhauser A, Morrison JC, Prediction of small for gestational age newborns using ultrasound estimated and actual amniotic fluid volume: Published data revisited, Aust. N. Z. J. Obstet. Gynaecol 48 (2008) 160–164. 10.1111/j.1479-828X.2008.00830.x. [PubMed: 18366489]

[3]. Figueras F, Eixarch E, Gratacos E, Gardosi J, Predictiveness of antenatal umbilical artery Doppler for adverse pregnancy outcome in small-for-gestational-age babies according to customised birthweight centiles: Population-based study, BJOG. 115 (2008) 590–594. 10.1111/j.1471-0528.2008.01670.x. [PubMed: 18333939]

[4]. Ingram E, Morris D, Naish J, Myers J, Johnstone E, MR Imaging Measurements of Altered Placental Oxygenation in Pregnancies Complicated by Fetal Growth Restriction, Radiology. 285 (2017) 953–960. 10.1148/radiol.2017162385. [PubMed: 28708473]

[5]. Luo J, Abaci Turk E, Bibbo C, Gagoski B, Roberts DJ, Vangel M, Tempany-Afdhal CM, Barnewolt C, Estroff J, Palanisamy A, Barth WH, Zera C, Malpica N, Golland P, Adalsteinsson E, Robinson JN, Grant PE, In Vivo Quantification of Placental Insufficiency by BOLD MRI: A Human Study, Sci. Rep 7 (2017) 3713. 10.1038/s41598-017-03450-0. [PubMed: 28623277]

[6]. Sørensen A, Peters D, Simonsen C, Pedersen M, Stausbøl-grøn B, Christiansen OB, Lingman G, Uldbjerg N, Changes in human fetal oxygenation during maternal hyperoxia as estimated by BOLD MRI, Prenatal Diagnosis. (2013). 10.1002/pd.4025.

[7]. Sørensen A, Sinding M, Peters DA, Petersen A, Frøkjær JB, Christiansen OB, Uldbjerg N, Placental oxygen transport estimated by the hyperoxic placental BOLD MRI response, (2015) 1–8. 10.14814/phy2.12582.

[8]. Sinding M, Peters DA, Poulsen SS, Frøkjær JB, Christiansen OB, Petersen A, Uldbjerg N, Sørensen A, Placental baseline conditions modulate the hyperoxic BOLD-MRI response, Placenta. 61 (2018) 17–23. 10.1016/j.placenta.2017.11.002. [PubMed: 29277267]

[9]. Sørensen A, Hutter J, Seed M, Grant PE, Gowland P, T2* weighted placental MRI: basic research tool or an emerging clinical test of placental dysfunction?, Ultrasound Obstet. Gynecol (2019). 10.1002/uog.20855.

[10]. Buxton RB, Dynamic models of BOLD contrast, Neuroimage. 62 (2012) 953–961. 10.1016/j.neuroimage.2012.01.012. [PubMed: 22245339]

[11]. Ma Y, Berman AJL, Pike GB, The effect of dissolved oxygen on the relaxation rates of blood plasma: Implications for hyperoxia calibrated BOLD, Magn. Reson. Med 76 (2016) 1905–1911. 10.1002/mrm.26069. [PubMed: 26628286]

[12]. Portnoy S, Seed M, Sled JG, Macgowan CK, Non-invasive evaluation of blood oxygen saturation and hematocrit from T 1 and T 2 relaxation times: In-vitro validation in fetal blood, Magn. Reson. Med 78 (2017) 2352–2359. 10.1002/mrm.26599. [PubMed: 28191646]

[13]. Portnoy S, Milligan N, Seed M, Sled JG, Macgowan CK, Human umbilical cord blood relaxation times and susceptibility at 3 T, Magn. Reson. Med 79 (2018) 3194–3206. 10.1002/mrm.26978. [PubMed: 29067745]

[14]. Portnoy S, Osmond M, Zhu MY, Seed M, Sled JG, Macgowan CK, Relaxation properties of human umbilical cord blood at 1.5 Tesla, Magn. Reson. Med 77 (2017) 1678–1690. 10.1002/mrm.26231. [PubMed: 27059881]

[15]. Liu P, Chalak LF, Krishnamurthy LC, Mir I, Peng S-L, Huang H, Lu H, T1 and T2 values of human neonatal blood at 3 Tesla: Dependence on hematocrit, oxygenation, and temperature, Magn. Reson. Med 75 (2016) 1730–1735. 10.1002/mrm.25775. [PubMed: 25981985]

[16]. Huen I, Morris DM, Wright C, Parker GJM, Sibley CP, Johnstone ED, Naish JH, R1 and R2* changes in the human placenta in response to maternal oxygen challenge, Magn. Reson. Med 70 (2013) 1427–1433. 10.1002/mrm.24581. [PubMed: 23280967]

[17]. Wright C, Morris DM, Baker PN, Crocker IP, Gowland PA, Parker GJ, Sibley CP, Magnetic resonance imaging relaxation time measurements of the placenta at 1.5 T, Placenta. 32 (2011) 1010–1015. 10.1016/j.placenta.2011.07.008. [PubMed: 21978937]

[18]. Rodríguez-Soto AE, Langham MC, Abdulmalik O, Englund EK, Schwartz N, Wehrli FW, MRI quantification of human fetal O2delivery rate in the second and third trimesters of pregnancy, Magn. Reson. Med 80 (2018) 1148–1157. 10.1002/mrm.27094. [PubMed: 29359353]

[19]. Ma D, Gulani V, Seiberlich N, Liu K, Sunshine JL, Duerk JL, Griswold MA, Magnetic resonance fingerprinting, Nature. 495 (2013) 187–192. 10.1038/nature11971. [PubMed: 23486058]

[20]. Rodríguez-Soto AE, Abdulmalik O, Langham MC, Schwartz N, Lee H, Wehrli FW, T2-prepared balanced steady-state free precession (bSSFP) for quantifying whole-blood oxygen saturation at 1.5T, Magn. Reson. Med 00 (2017) 1–8. 10.1002/mrm.26835.

[21]. Jiang Y, Ma D, Seiberlich N, Gulani V, Griswold M. a., MR fingerprinting using fast imaging with steady state precession (FISP) with spiral readout, Magn. Reson. Med 74 (2015) 1621–1631. 10.1002/mrm.25559. [PubMed: 25491018]

[22]. Gagoski B, Ye H, Cauley S, Bhat H, Setsompop K, Chatnuntawech I, Martin A, Jiang Y, Griswold M, Adalsteinsson E, Grant PE, Wald L, Magnetic resonance fingerprinting for fetal imaging at 3T - intial results, in: Proc. Intl. Soc. Mag. Reson. Med, 2015: p. 3429.

[23]. Cao X, Liao C, Wang Z, Chen Y, Ye H, He H, Zhong J, Robust sliding-window reconstruction for Accelerating the acquisition of MR fingerprinting, Magn. Reson. Med 00 (2016) 1–10. 10.1002/mrm.26521.

[24]. Spatz M, Garcia-Polo P, Keil B, Ha C, Wald LL, A 64 channel 3T array coil for highly accelerated fetal imaging at 22 weeks of pregnancy, in: Proc. Intl. Soc. Mag. Reson, 2017: p. 1220.

[25]. Nelson DM, Burton GJ, A technical note to improve the reporting of studies of the human placenta, Placenta. 32 (2011) 195–196. 10.1016/j.placenta.2010.12.008. [PubMed: 21239055]

[26]. Keenan KE, Stupic KF, Boss MA, Russek SE, Chenevert TL, Prasad PV, Reddick WE, Cecil KM, Zheng J, Hu P, Jackson EF, Multi-site, multi-vendor comparison of T1 measurement using ISMRM/NIST system phantom, in: Proc. Int. Soc. Magn. Reson. Med, Singapore, 2016: p. 3290.

[27]. Jiang Y, Ma D, Keenan KE, Stupic KF, Gulani V, Griswold MA, Repeatability of magnetic resonance fingerprinting T1 and T2 estimates assessed using the ISMRM/NIST MRI system phantom, Magn. Reson. Med 00 (2016) 1–6. 10.1002/mrm.26509.

[28]. Chung S, Kim D, Breton E, Axel L, Rapid B1+ mapping using a preconditioning RF pulse with turboFLASH readout, Magn. Reson. Med 64 (2010) 439–446. 10.1002/mrm.22423. [PubMed: 20665788]

[29]. Barral JK, Gudmundson E, Stikov N, Etezadi-Amoli M, Stoica P, Nishimura DG, A robust methodology for in vivo T1 mapping, Magn. Reson. Med 64 (2010) 1057–1067. 10.1002/mrm.22497. [PubMed: 20564597]

[30]. Weigel M, Extended phase graphs: dephasing, RF pulses, and echoes - pure and simple, J. Magn. Reson. Imaging 41 (2015) 266–295. 10.1002/jmri.24619. [PubMed: 24737382]

[31]. Poorman ME, Martin MN, Ma D, McGivney DF, Gulani V, Griswold MA, Keenan KE, Magnetic resonance fingerprinting Part 1: Potential uses, current challenges, and recommendations, J. Magn. Reson. Imaging 51 (2020) 675–692. 10.1002/jmri.26836. [PubMed: 31264748]

[32]. Chen Y, Jiang Y, Pahwa S, Ma D, Lu L, Twieg MD, Wright KL, Seiberlich N, Griswold MA, Gulani V, MR Fingerprinting for Rapid Quantitative Abdominal Imaging, Radiology. 279 (2016) 278–286. 10.1148/radiol.2016152037. [PubMed: 26794935]

[33]. Ma D, Coppo S, Chen Y, McGivney DF, Jiang Y, Pahwa S, Gulani V, Griswold MA, Slice profile and B1corrections in 2D magnetic resonance fingerprinting, Magn. Reson. Med 78 (2017) 1781–1789. 10.1002/mrm.26580. [PubMed: 28074530]

[34]. Ingram E, Hawkins L, Morris DM, Myers J, Sibley CP, Johnstone ED, Naish JH, R1 changes in the human placenta at 3 T in response to a maternal oxygen challenge protocol, Placenta. 39 (2016) 151–153. 10.1016/j.placenta.2016.01.016. [PubMed: 26992688]

[35]. Gowland PA, Freeman A, Issa B, Boulby P, Duncan KR, Moore RJ, Baker PN, Bowtell RW, Johnson IR, Worthington BS, In vivo relaxation time measurements in the human placenta using echo planar imaging at 0.5 T, Magn. Reson. Imaging 16 (1998) 241–247. 10.1016/S0730-725X(97)00308-1. [PubMed: 9621965]

[36]. Derwig I, Barker GJ, Poon L, Zelaya F, Gowland P, Lythgoe DJ, Nicolaides K, Association of placental T2 relaxation times and uterine artery Doppler ultrasound measures of placental blood flow, Placenta. 34 (2013) 474–479. 10.1016/j.placenta.2013.03.005. [PubMed: 23583071]

[37]. Stanisz GJ, Odrobina EE, Pun J, Escaravage M, Graham SJ, Bronskill MJ, Henkelman RM, T1, T2 relaxation and magnetization transfer in tissue at 3T, Magn. Reson. Med 54 (2005) 507–512. 10.1002/mrm.20605. [PubMed: 16086319]

[38]. Soothill PW, Nicolaides KH, Rodeck CH, Campbell S, Effect of gestational age on fetal and intervillous blood gas and acid-base values in human pregnancy, Fetal Ther. 1 (1986) 168–175. 10.1159/000262264. [PubMed: 3454532]

[39]. Boxerman JL, Hamberg LM, Rosen BR, Weisskoff RM, MR contrast due to intravascular magnetic susceptibility perturbations, Magn. Reson. Med 34 (1995) 555–566. 10.1002/mrm.1910340412. [PubMed: 8524024]

[40]. Porayette P, Sun L, Jaeggi E, Grosse-Wortmann L, Yoo S-J, Hickey E, Miller S, Macgowan C, Seed M, MRI reveals hemodynamic changes with acute maternal hyperoxygenation in human fetuses with and without congenital heart disease, J. Cardiovasc. Magn. Reson 17 (2015) O55. 10.1186/1532-429X-17-S1-O55.

[41]. Chuai Y, Jiang W, Xu X, Wang A, Yao Y, Chen L, Maternal oxygen exposure may not change umbilical cord venous partial pressure of oxygen: non-random, paired venous and arterial samples from a randomised controlled trial, BMC Pregnancy Childbirth. 20 (2020) 510. 10.1186/s12884-020-03212-3. [PubMed: 32887557]

[42]. Silvennoinen MJ, Kettunen MI, Kauppinen RA, Effects of hematocrit and oxygen saturation level on blood spin-lattice relaxation, Magn. Reson. Med 49 (2003) 568–571. 10.1002/mrm.10370. [PubMed: 12594761]

[43]. Davis L, Placental Respiratory Gas Exchange, Anesthesia and the Fetus. (2012) 25–31. 10.1002/9781118477076.ch3.

[44]. Tadamura E, Hatabu H, Li W, Prasad PV, Edelman RR, Effect of oxygen inhalation on relaxation times in various tissues, J. Magn. Reson. Imaging 7 (1997) 220–225. 10.1002/jmri.1880070134. [PubMed: 9039619]

[45]. Stout JN, Rouhani S, Liao C, Turk EA, Ha CG, Rich K, Wald LL, Barth WHJ, Roberts DJ, Adalsteinsson E, Grant PE, Placental MRI: Using a novel ex vivo placental perfusion chamber to validate in vivo magnetic resonance fingerprinting (MRF) relaxometry, in: Proc Intl Soc Mag Reson Med 28, Virtual, 2020: p. 580.

[46]. Hamilton JI, Jiang Y, Chen Y, Ma D, Lo WC, Griswold M, Seiberlich N, MR fingerprinting for rapid quantification of myocardial T1, T2, and proton spin density, Magn. Reson. Med 77 (2017) C1. 10.1002/mrm.26668.

[47]. Yu Z, Zhao T, Assländer J, Lattanzi R, Sodickson DK, Cloos MA, Exploring the sensitivity of magnetic resonance fingerprinting to motion, Magn. Reson. Imaging 54 (2018) 241–248. 10.1016/j.mri.2018.09.002. [PubMed: 30193953]

[48]. Xu Z, Ye H, Lyu M, He H, Zhong J, Mei Y, Chen Z, Wu EX, Chen W, Feng Q, Feng Y, Rigid motion correction for magnetic resonance fingerprinting with sliding-window reconstruction and image registration, Magn. Reson. Imaging (2018). 10.1016/j.mri.2018.11.001.

[49]. Mehta BB, Ma D, Pierre EY, Jiang Y, Coppo S, Griswold MA, Image reconstruction algorithm for motion insensitive MR Fingerprinting (MRF): MORF, Magn. Reson. Med (2018) 1–16. 10.1002/mrm.27227.

[50]. Hamilton JI, Jiang Y, Ma D, Lo WC, Gulani V, Griswold M, Seiberlich N, Investigating and reducing the effects of confounding factors for robust T1and T2mapping with cardiac MR fingerprinting, Magn. Reson. Imaging 53 (2018) 40–51. 10.1016/j.mri.2018.06.018. [PubMed: 29964183]

[51]. Liao C, Bilgic B, Manhard MK, Zhao B, Cao X, Zhong J, Wald LL, Setsompop K, 3D MR fingerprinting with accelerated stack-of-spirals and hybrid sliding-window and GRAPPA reconstruction, Neuroimage. 162 (2017) 13–22. 10.1016/j.neuroimage.2017.08.030. [PubMed: 28842384]

[52]. Cao X, Ye H, Liao C, Li Q, He H, Zhong J, Fast 3D brain MR fingerprinting based on multi-axis spiral projection trajectory, Magn. Reson. Med (2019) 1–13. 10.1002/mrm.27726.

[53]. Ma D, Jiang Y, Chen Y, McGivney D, Mehta B, Gulani V, Griswold M, Fast 3D magnetic resonance fingerprinting for a whole-brain coverage, Magn. Reson. Med 79 (2018) 2190–2197. 10.1002/mrm.26886. [PubMed: 28833436]

[54]. Wang F, Dong Z, Reese TG, Bilgic B, Katherine Manhard M, Chen J, Polimeni JR, Wald LL, Setsompop K, Echo planar time-resolved imaging (EPTI), Magn. Reson. Med 81 (2019) 3599–3615. 10.1002/mrm.27673. [PubMed: 30714198]

[55]. Manhard MK, Liao C, Stockmann J, Park D, Han S, Polimeni J, Bilgic B, Setsompop K, Combined T1 , T2 , and T2* mapping using a multi-inversion multi-echo spin and gradient echo EPI sequence, in: Proc 27th Annual Meeting ISMRM, 2019.

[56]. Hutter J, Jackson L, Ho A, Pietsch M, Story L, Chappell LC, Hajnal JV, Rutherford M, T2* relaxometry to characterize normal placental development over gestation in-vivo at 3T, Wellcome Open Res. 4 (2019) 166. 10.12688/wellcomeopenres.15451.1.

[57]. Melbourne A, Aughwane R, Sokolska M, Owen D, Kendall G, Flouri D, Bainbridge A, Atkinson D, Deprest J, Vercauteren T, David A, Ourselin S, Separating fetal and maternal placenta circulations using multiparametric MRI, Magn. Reson. Med 81 (2019) 350–361. 10.1002/mrm.27406. [PubMed: 30239036]

[58]. Abaci Turk E, Abulnaga SM, Luo J, Stout JN, Feldman HA, Turk A, Gagoski B, Wald LL, Adalsteinsson E, Roberts DJ, Bibbo C, Robinson JN, Golland P, Grant PE, Barth WH Jr, Placental MRI: Effect of maternal position and uterine contractions on placental BOLD MRI measurements, Placenta. 95 (2020) 69–77. 10.1016/j.placenta.2020.04.008. [PubMed: 32452404]

[59]. Pauly J, Le Roux P, Nishimura D, Macovski A, Parameter relations for the Shinnar-Le Roux selective excitation pulse design algorithm [NMR imaging], IEEE Trans. Med. Imaging 10 (1991) 53–65. 10.1109/42.75611. [PubMed: 18222800]

Highlights

- Performance of a 9-second MRF acquisition was tested on anatomically correct phantoms
- Placental T_1 and T_2 maps were acquired for 31 pregnant women before and during hyperoxia
- Changes in placental T_2 were detected during maternal hyperoxia consistent with increased placental oxygenation

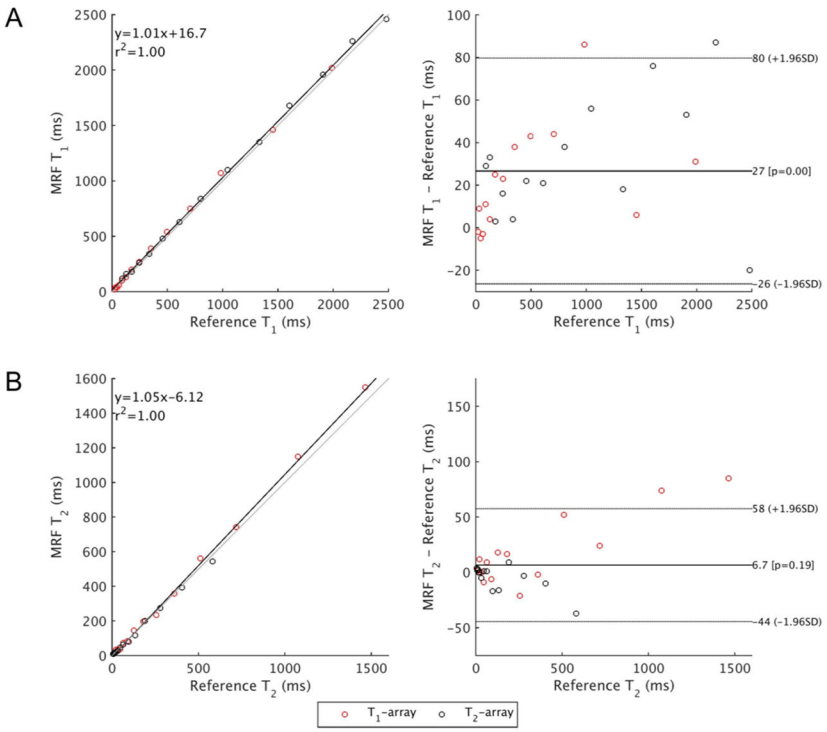

Figure 1.

Bland-Altman analysis of relaxation times of the T_1- and T_2-arrays of the NIST phantom. MRF values have been corrected for B_1^+ and slice profile effects, and the median value from within the manual ROI is shown here. NIST relaxation times are published reference values [26].

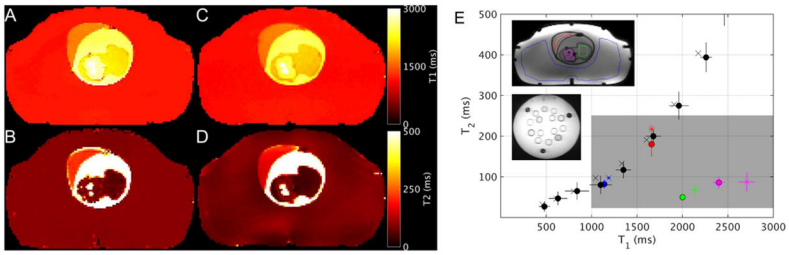

Figure 2.

T_1 (A, C) and T_2 (B, D) maps from the 22 week phantom determined by reference techniques (A, B) and by MRF (C, D). T_2 versus T_1 values for NIST and 22-week phantom (E). The symbol marks the median parameter value and the error bars show IQR of the voxels within the hand-drawn ROI. The ROIs are represented by color and shown in the inset: NIST phantom T_2-array (black), abdomen (blue), placenta (red), fetal body (green), and fetal brain (magenta). The measurement types are represented by symbols: reference or ground truth (x) and B_1^+ and slice profile corrected MRF (circle). The gray rectangle indicates the relaxation time range expected in fetal tissues.

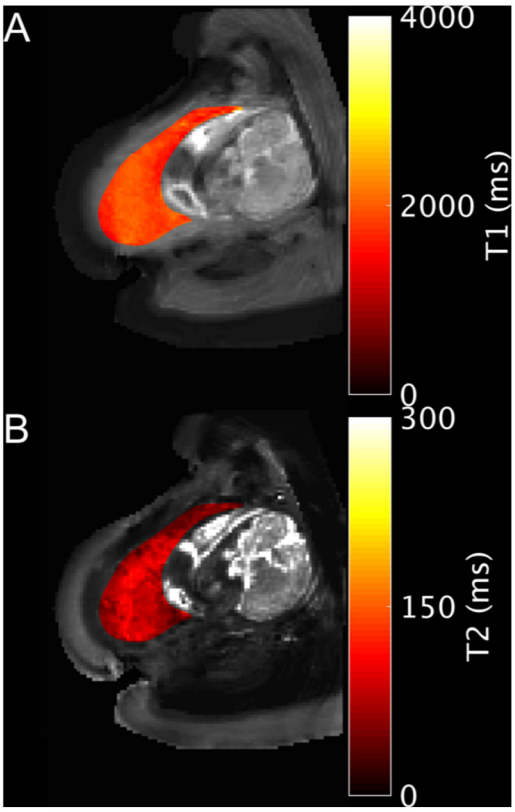

Figure 3.

Example T_1 (A) and T_2 (B) parameter maps for the placenta of subject 20 (34w). Acquisition was in the transverse plane while the subject was in the left lateral position.

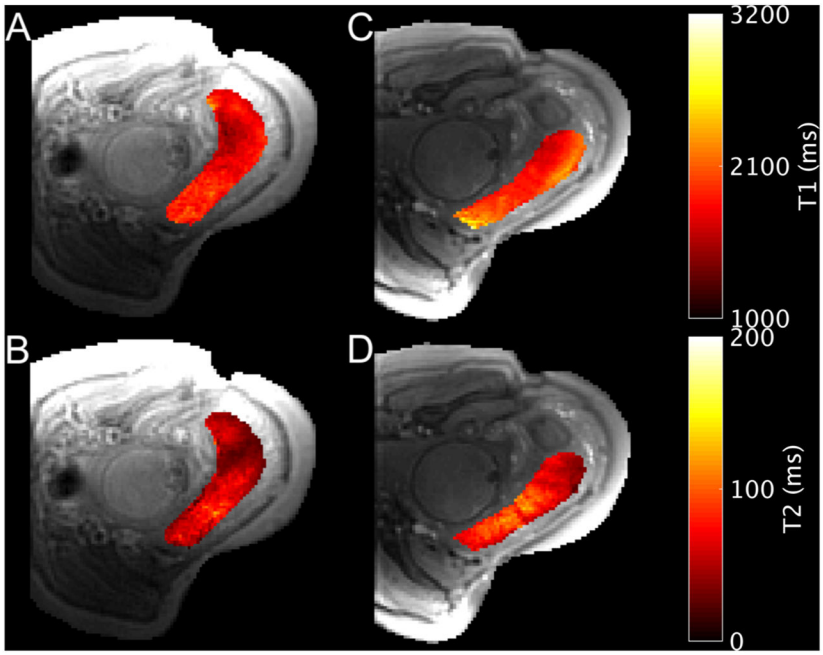

Figure 4.

Example T_1 (A, C) and T_2 (B, D) parameter maps during normoxia (A, B) and hyperoxia (C, D) for the placenta of subject 31 (31w4d). Acquisition was in the transverse plane while the subject was in the left lateral position. The imaging plane shifted due to maternal and fetal motion between normoxia and hyperoxia.

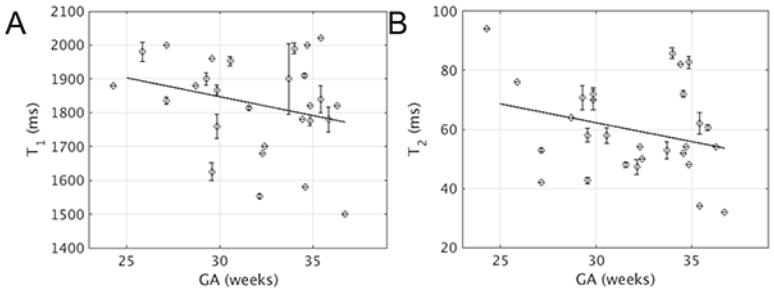

Figure 5.

Scatter plots of median T_1 (A) or T_2 (B) across the placental ROI versus GA for all motion free scans during normoxia. Error bars indicate same-subject standard deviation for multiple measurements, which is possibly zero for subjects with only one measurement. Both linear regression lines are statistically insignificant (T_1: $R^2 = 0.04$, $P = 0.16$; T_2: $R^2 = 0.04$, $P = 0.15$).

Table 1:

Clinical characteristics of pregnancies for placentas studied [25]

Parameter			
Gravidity	Median = 2	25-75% = 2-3	Range = 1-9
Parity	Median = 0	25-75% = 0-1	Range = 0-3
Gestational age at delivery (weeks)	Average = 38.7	SD = 2.4	Range = 30.29-41.14
Gestational age at scan (weeks)	Average = 32	SD = 3.3	Range = 24.29-36.71
Maternal age (years)	Average = 34.4	SD = 5.63	Range = 24 −47
Race	Unknown		
Ethnicity	Unknown		
Prenatal medications	Unknown		
Drugs	Unknown		
Previous prenatal admission(s)	Unknown		
Blood pressures <140/90 mm Hg	Yes, n = 3	No, n = 13	Unknown = 15
Screened for diabetes	Yes = 2	No = 14	Unknown = 15
	Unknown		
Beta strep status	Unknown		
Antenatal steroids:	Unknown		
Magnesium sulfate	Unknown		
Anesthesia	Unknown		
Cervical ripening agent	Unknown		
Labor	Unknown		
Delivery mode (N= # patients)	Unknown		
Maternal Oxygen given at delivery?	Yes, n = 0	No, n = 18	Unknown = 15
Birth weight (grams)	Average = 3300	SD = 378	Unknown = 9
Placental weight (grams)	Unknown		
Baby's sex	Female = 15	Male = 13	Unknown = 4
Delivery to processing (mins)	Unknown		

Table 2:

Results from mixed-effects modeling of the median and IQR of parameter values within the placenta ROI with fixed effects for oxygen state (α_{O2}), linear effect for gestational age (β), and a random effect for subject identification to account for within-subject correlation in those with multiple measurements. Results affected by motion were excluded a priori in four models, but included for two models where an additional fixed effect for motion (α_{motion}) was used to assess its effect on T_1 and T_2 estimates in vivo. Subject counts in the final column are counted in total, for subjects with both air and O_2 measurements, and for total subjects with air and O_2 measurements.

	Fixed effects coefficients (estimate±SE)				**Random effects covariance (std, 95%CI)**		
Response Variable	**Intercept**	**α_{O2}**	**β_{GA}**	**α_{motion}**	**Subject**	**Error**	**N subjects (total/ both/air/O2)**
Median T_1 motion excluded	**2051.20±237.25, P=1.4e-14**	6.68±12.14, P=0.58	−7.00±7.39, P=0.34		125.73 (95.22, 166.00)	65.19 (57.07, 74.46)	29/21/28/22
Median T_2 motion excluded	**88.31±24.25, P=0.00039**	**2.87±1.38, P=0.039**	−0.82±0.75, P=0.28		12.68 (9.55, 16.83)	7.42 (6.50, 8.47)	
T_1 IQR motion excluded	**412.08±146.61, P=0.0057**	**−26.81±10.32, P=0.01**	−6.84±4.56, P=0.14		73.75 (55.39, 98.21)	55.75 (48.89, 63.58)	
T_2 IQR motion excluded	**27.66±2.71, P=0.031**	1.25±0.71, P=0.082	−0.14±0.40, P=0.72		6.66 (5.00, 8.87)	3.83 (3.35, 4.37)	
Median T_1	**2025.93±238.75, P=5.6e-15**	−2.16±10.40, P=0.84	−6.50±7.41, P=0.38	3.90±12.95, P=0.76	129.83 (99.52, 169.39)	68.52 (61.53, 76.31)	31/27/31/27
Median T_2	**97.56±24.41, P=9.1e-05**	**2.79±1.30, P=0.034**	−1.11 ±0.76, P=0.14	**−10.04±1.62, P=3.3e-09**	13.01 (9.92, 17.05)	8.61 (7.73, 9.59)	